Estimation of joint contact pressure in the index finger using a hybrid finite element musculoskeletal approach

Barthélémy Faudot, Jean-Louis Milan, Benjamin Goislard de Monsabert, Thomas Le Corroller, Laurent Vigouroux

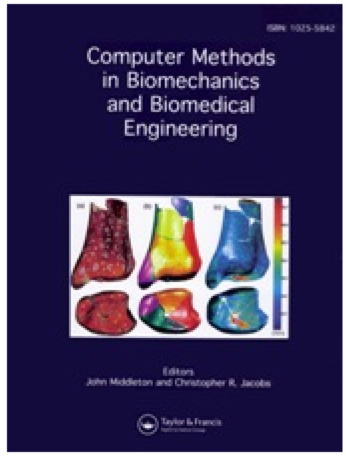

Estimation of joint contact pressure in the index finger using a hybrid finite element musculoskeletal approach

Journal:	*Computer Methods in Biomechanics and Biomedical Engineering*
Manuscript ID	GCMB-2020-0028
Manuscript Type:	Research Article (4,000 words)
Date Submitted by the Author:	17-Jan-2020
Complete List of Authors:	Faudot, Barthélémy; Aix-Marseille Universite, Institute of Movement Sciences Milan, Jean-Louis; Aix-Marseille Universite, Institute of Movement Sciences Goislard de Monsabert, Benjamin; Aix-Marseille Universite, Institute of Movement Sciences Le Corroller, Thomas; Aix-Marseille Universite, Institute of Movement Sciences; Assistance Publique Hopitaux de Marseille, Institute for Locomotion - Department of Radiology - St Marguerite Hospital Vigoroux, Laurent; Aix-Marseille Universite, Institute of Movement Sciences
Keywords:	Hand biomechanics, joint contact pressure, pinch grip task, finite element analysis, musculoskeletal model

Estimation of joint contact pressure in the index finger using a hybrid finite element musculoskeletal approach

Barthélémy Faudot[a]*, Jean-Louis Milan[a], Benjamin Goislard de Monsabert[a], Thomas Le Corroller[a,b], Laurent Vigouroux[a]

[a]*Aix Marseille University, CNRS, ISM, Marseille, France*
[b]*APHM, Institute for Locomotion, Department of Radiology, St Marguerite Hospital, Marseille, France*

*Corresponding Author
Barthélémy Faudot
Faculty of Sport Science, CP 910
Institute of Movement Science
163 Avenue de Luminy
13288 Marseille Cedex 09 (France)
Email: barthelemy.faudot@univ-amu.fr
Tel: +33(0)4 91 75 96 55
Fax: +33(0)4 91 17 22 52

Estimation of joint contact pressure in the index finger using a hybrid finite element musculoskeletal approach

Abstract

The knowledge of local stress distribution in hand joints, in particular joint contact pressure, is crucial to understand injuries and osteoarthritis occurrence. However, determining cartilage contact stresses remains a challenge, requiring numerical models including both accurate anatomical components and realistic tendon force actuation. Contact forces in finger joints have frequently been calculated but little data is available on joint contact pressures. This study aimed to develop and validate a hybrid biomechanical model of the index finger to estimate in-vivo joint contact pressure during a static maximal strength pinch grip task. The hybrid model employed a two-step approach. First, a three-dimensional finite element model including bones, cartilage, tendons and ligaments was developed, with tendon force transmission based on a tendon-pulley system. Then, this model was driven by realistic tendon forces estimated from a musculoskeletal model and motion capture data for six subjects. The hybrid model outputs agreed well with experimental measurement of fingertip forces and musculoskeletal model results. Mean contact pressures were 8.0±1.4 MPa, 7.0±1.3 MPa and 7.2±2.6 MPa for metacarpophalangeal, proximal and distal interphalangeal joints, respectively. Two subjects had higher mean contact pressure in the distal joint than in the two other joints, suggesting a mechanical cause for the prevalence of osteoarthritis in the index distal joint. This first application of an effective hybrid model to the index finger holds promise for estimating hand joint stresses under common daily grip tasks. Knowledge of comprehensive hand biomechanics is of major clinical interest to provide the numerical groundwork to improve surgical procedures.

Keywords

Hand biomechanics, joint contact pressure, pinch grip task, finite element analysis, musculoskeletal model

Introduction

The human hand is a sophisticated biological tool involved in numerous everyday activities (Bardo et al. 2018). The gripping tasks performed by the hand are essential for most movements in daily and working life. One of the commonest of the various techniques (e.g.: cylindrical, key pinch, hook grip) (Napier 1956) used to manipulate objects is the pinch grip, which consists in holding an object between the thumb and the index fingertips (Vergara et al. 2014). Because of its specific biomechanical configuration, this grip technique can lead to high joint loadings that expose the fingers to injuries such as rheumatoid arthritis and osteoarthritis (OA) (Jensen et al. 1999; McQuillan et al. 2016). Cumulative excessive stress acting on normal joints has in fact been identified as one of the main risk factors for the development of OA (Guilak 2011; Buckwalter et al. 2013). Hence, quantifying the biomechanical stress distribution on the finger's musculoskeletal system, especially joint contact pressure, could provide a better understanding of joint disease (Goislard de Monsabert et al. 2014) and improve rehabilitation (Fowler & Nicol 2000; Completo et al. 2018).

Direct measurements of joint pressures have been estimated in-vivo using pressure sensors (Rikli et al. 2007) and instrumented prostheses for large joints (D'Lima et al. 2006). However, the highly invasive nature of such techniques makes them ethically questionable and a technical challenge, especially when applied to the small finger joints. Only a few in vitro experimental data for the hand are available, due to the joint size and to the surrounding tissues that complicate the insertion of such sensors. Therefore, computational modelling, being non-invasive, appears to be the most suitable method of estimating joint mechanics.

Finite element (FE) and musculoskeletal (MSK) are the main modelling approaches currently used to study joint loadings (Henak et al. 2013). They have been widely applied to the lower limb during isometric tasks (Cheung et al. 2005) and gait locomotion (Andriacchi et al. 2009) to estimate either joint kinematics, reaction forces or joint cartilage stress. Due to the number of anatomical components involved and the complexity of soft-tissue interaction, multi-articular systems such as the finger, wrist or ankle have received less attention. Most hand biomechanical models use an MSK representation for either the index finger (Fowler & Nicol 2000; Synek & Pahr 2016), the thumb-index pinch complex (Barry et al. 2018) or the entire hand (Goislard de Monsabert et al. 2014). Although such models provide estimations of tendon forces and resultant joint contact forces, they neglect the non-linear deformation of soft tissues and the local stress distribution. Conversely, FE hand models provide estimations of local contact mechanics but focus on a single joint (Hashizume et al. 1994), model joints in 2D (Butz et al. 2012a), neglect muscle actions and tendon paths (Butz et al. 2012b) and apply non-physiological boundary conditions (Harih 2019). To take advantage of both approaches, hybrid MSK-FE models have been developed to investigate different musculoskeletal structures, such as the wrist (Gíslason et al. 2010), the ankle (Wang et al. 2016) or the knee (Besier et al. 2005; Halonen et al. 2017). However, the implementation of this hybrid approach remains challenging when modelling the hand, whose multi-joint configuration makes it particularly difficult to validate the numerical procedure.

A hybrid MSK-FE model representing bones, cartilage, tendons, annular pulleys and ligaments while considering the multi-joint actions of tendons would help to improve the understanding of musculoskeletal diseases. To the best of our knowledge, no studies have so far applied this hybrid approach to the hand joints. Thus, the purpose of this paper was to provide a validated hybrid biomechanical model of the index finger that estimates in-vivo joint contact pressure by applying realistic muscle actions during a static maximal strength pinch grip task.

Methods

The workflow of the study is presented in Fig. 1. This hybrid approach combined an already published MSK model based on experimental data with a newly developed FE model of the index finger based on medical imaging and literature data. The MSK model estimated tendon forces from kinematic and force data through an inverse dynamic approach. Tendon forces were then inputted into the FE model and joint contact pressures were computed.

[Figure 1 about here]

Experimental kinematic and force data

The experimental setup and protocol already reported (Goislard de Monsabert et al. 2014) are briefly described here. Ten healthy right-handed males free of upper extremity disorders were recruited (age: 25.5±3.2 years; height: 178.6±6.1 cm; weight: 71.2±7.2 kg; hand length: 19.0±0.8 cm). Kinematic and force data (Fig. 2) were simultaneously recorded. A six-axial force sensor (Nano-25; ATI Industrial Automation, USA) 5.5 cm long was used to record the force applied by the thumb and index fingertips. The 3D position of hand segments was tracked using spherical reflecting markers and a six-camera optoelectronic system (MX T40; Vicon, UK). Joint angles and the three grip force components were then inputted into the MSK model.

[Figure 2 about here]

Tendon force estimation using a musculoskeletal model

A full description of the MSK model is provided in a previous study (Goislard de Monsabert et al. 2012). The model estimated 42 tendon forces to balance 23 degrees of freedom (DoF) representing the five fingers and the wrist. The segments were modelled as rigid bodies articulated by sixteen frictionless joints. In the first step, the 42 tendon forces required to balance external forces were estimated using a static optimisation to solve the muscular redundancy problem. In the second step, joint reaction forces were derived from tendon and external fingertip forces using the force equilibrium equation.

Finite element model

Model geometry

A healthy male subject free of upper extremity disorders was recruited to acquire computed tomography (CT) images of the right hand (age: 37 years; height: 185 cm; weight: 74 kg; hand length: 19.7 cm). The participant signed an informed consent form and the protocol was approved by the local ethics committee. The CT system was a LightSpeed VCT (GE Medical Systems, USA) (150 mA x 120 kV; slice thickness 625 µm; pixel size 325 µm). The subject placed his hand in a semi-rigid cast that constrained him in a pinch grip posture. The cast was made prior to the acquisition to avoid any effect of fatigue. Polyurethane resin tapes (Soft Cast, 3M, USA) were positioned while the subject was holding a 5.5 cm-long tube, i.e. the same length as the force sensor.

Segmentation of bones was performed from the CT-scan acquisition using the 3D image reconstruction software Mimics (Research 20.0; Materialise, Belgium). Index phalanges and truncated metacarpal bone were meshed using quadratic tetrahedral elements (C3D10) with a maximum element edge length of 1.5 mm. Solid geometries were imported into Abaqus (2018; Simulia, USA). The cartilage was manually created by identifying joint surfaces on bones and then extruding surface elements to form two-layer wedge elements (C3D6), each of whose widths equalled half the minimum distance between bones (Anderson et al. 2010). Cartilage distribution and thickness (from 0.4 to 0.8 mm) were compared against literature values (Robson et al. 1995). The FE model's total number of elements was roughly 200 000.

Modelling tissue properties

Finger bones were modelled as a linear elastic isotropic material, distinguishing between cortical (E=18 GPa, ν=0.2) and cancellous bone (E=300 MPa, ν=0.25) (Rho et al. 1997), see Fig. 3(B). Cartilage was modelled using a 3rd order Ogden hyper-elastic material as detailed in Table 1. Supplementary analysis was performed to investigate the effect of bone material properties on the model results.

All the tendons and muscles involved in index finger function were modelled: *terminal extensor*, *flexor digitorum profundus* (FDP) at distal interphalangeal (DIP) joint, *extensor slip*, *radial band*, *ulnar band*, *flexor digitorum superficialis* (FDS) at proximal interphalangeal (PIP) joint and *long extensor* (considering both *extensor digitorum communis* (EDC) and *extensor digitorum indicis* (EDI)), *radial interosseus* (RI), *ulnar interosseus* (UI), *lumbrical* (LU) at metacarpophalangeal (MCP) joint. The paths of these tendons were determined by the same anatomical and geometrical data in the MSK model and scaled according to phalange dimensions (An et al. 1979). Each tendon was modelled using straight beams (B31) to connect the points given by the anatomical dataset, i.e. two points at each joint. Tendons were held tight to the bone by annular pulleys modelled with shell elements (S4) for both flexor and extensor tendons (see Fig. 3).

Collateral ligaments and volar plates were modelled as the main stabilisers of the index finger joints (Minami et al. 1985). The same attachment points as those used for the MSK model were estimated from an anatomical study (An et al. 1979). Distributed insertions were simulated by applying ligaments in parallel at adjacent node points on the bone surface. Ligaments were modelled as non-linear spring elements (CONN3D2) with tension-only behaviour and pre-strain at initial length (Rhee et al. 1992). Model values are summarised in Table 1.

[Table 1 about here]

[Figure 3 about here]

Loads and boundary conditions

Loadings on the hybrid model were driven through the estimation of tendon forces provided by the MSK analysis previously described. Four of the ten subjects were excluded from the analysis due to the large difference between their joint angles and those of the scanned subject. For the six remaining subjects, tendon forces were applied to the end of each tendon in the direction of the last beam segment (Fig. 3) and the six datasets were analysed. An extra simulation was performed using the average value of tendon forces. Supplementary analysis was also conducted to investigate the effect of tendon forces on the model results.

Bone and cartilage were fixed together so as to allow no relative motion between them. A friction coefficient of 0.02 (Wright & Dowson 1976) was applied to each cartilage joint surface. The proximal end of the truncated metacarpal bone was fully constrained and index fingertip nodes were restricted to one DoF to model the contact with the force sensor (see Fig. 3).

The Abaqus explicit solver was used for the analysis, this algorithm making the contact model robust.

Verification and validation of the hybrid model

To validate the hybrid approach, several analyses were performed to assess the quality of the hybrid model. First, the FE environment was evaluated through an assessment of the mesh quality and the convergence criterion. Resultant fingertip forces estimated in the hybrid model at the fixed fingertip nodes were compared to the experimental forces measured by the force sensor. The ratio of inputted tendon forces to estimated fingertip forces provided by the hybrid model for both FDP and FDS was compared to literature values. Lastly, the sum of reaction forces for all nodes of each joint in the hybrid model was compared to the joint reaction forces of the MSK model. These comparisons were performed using the average value of tendon forces of the six subjects inputted into the hybrid model.

Results

Results of the MSK model

The MSK model results are summarised here, for a full description see (Goislard de Monsabert et al. 2014). Tendon forces and averaged tendon force values for the six subjects are given in Supplementary Material A. For flexor tendons, resulting tensions were 158.0 ± 82.2 N and 109.8 ± 41.0 for the FDP and FDS tendons, respectively. For the extensor mechanism, resulting tensions were 5.1 ± 5.6 N, 181.2 ± 46.3 N, 0.0 ± 0.0 N, 85.6 ± 34.1 N, 110.0 ± 43.8 N for the LU, RI, UI, EDC and EDI tendons, respectively.

Subjects gripped the object using a variety of finger postures. DIP, PIP, and MCP flexion angles ranged from 8.9° to 28.8°, -1.0° to 21.3° and 46.5° to 64.4°, respectively. The scanned subject had flexion angles of 9.3°, 16.9°, and 47.6° for DIP, PIP and MCP joints, respectively.

Finite element environment quality indicators

Mesh quality was checked against the recommendations of a previously published article (Burkhart et al. 2013), detailed in Table 2, ensuring that elements with poor mesh metrics were located far from areas of interest. The model converged, at the end of the load step, with a mean kinetic energy of 3.4% of the total strain energy. Any dynamic behaviour was excluded according to the literature (Choi et al. 2002), leading to a quasi-static simulation.

[Table 2 about here]

Validation of the hybrid model

The hybrid model outputs agreed well with experimental and MSK model results. The fingertip reaction force estimated by the hybrid model using averaged tendon force was 54.8 N, lower than the experimental measurement by the force sensor, but remained within one standard deviation (66.2±13.3 N). The hybrid model estimated a tendon force to external fingertip force ratio of 1.85 and 2.67 for FDP and FDS, respectively, as shown in Table 3. The joint reaction forces estimated by the hybrid model were higher than those of the MSK model but remained within one standard deviation. The sum of DIP, PIP and MCP joint reaction forces was 758.2 N, 481.7 N and 248.7 N, respectively. The results are summarised in Table 4.

[Table 3 about here]

[Table 4 about here]

Joint mechanical stresses estimated by the hybrid model

Joint contact pressure on cartilage surfaces and Von Mises stress distribution on bones of the index finger during a pinch grip task for one dataset of tendon forces are displayed in Fig. 4. The highest stress was found on the surface of the metacarpal bone. High stress-intensity regions were visible at bone-pulley interface and at ligament insertions because of the node coupling points (Fig. 4). However, these stresses were highly localised and not representative of the real bone condition, being due to numerical artefacts. Finger joint contact areas were computed by summing all the facets bearing contact force and yielded 53.4±4.6 mm², 76.2±5.1 mm² and 94.8±2.1 mm² for DIP, PIP and MCP joints, respectively. Maximal contact pressure on cartilage was computed as well as mean contact pressure by averaging pressure values on the contact area at each joint (Fig.4). For DIP, PIP, and MCP joints, maximal contact pressure was 30.3±8.2 MPa, 31.9±8.8 MPa, and 33.8±6.9 MPa and mean contact pressure was 7.2±2.6 MPa, 7.0±1.3 MPa, and 8.0±1.4 MPa, respectively, as shown in Table 5.

[Table 5 about here]

[Figure 4 about here]

Sensitivity analysis

The sensitivity analysis on material properties showed that considering bones as rigid or homogeneous elastic solid tended to increase joint contact pressure. On sensitivity to tendon force, the results showed that joint contact pressure and external fingertip force decreased linearly with tendon force intensity. Further details can be found in Supplementary Material B.

Discussion

We described here the development of a hybrid biomechanical model of the index finger to estimate joint contact pressure during a static maximal strength pinch grip task in an FE environment driven by tendon forces calculated by an MSK model. This method combines two different numerical hand models to estimate joint mechanical stresses, notably mean and maximal joint contact pressures. This highly innovative approach represents, to the best of our knowledge, the first attempt to apply and validate a multi-articular hybrid model to the hand joints.

When evaluated through a combination of sensitivity analysis and comparison with experimental measurements, MSK results and literature data, the hybrid model was shown to provide realistic estimation of hand loadings. First, the estimated fingertip reaction force was in good agreement with the experimental grip force recorded using the force sensor, with only a 17% difference stable across subjects. The consistency of this gap suggests that its origin lies in the use of a single bone geometry in the hybrid model, whereas the experimental gripping task involved six subjects, each with a different bone geometry. There was good agreement in resultant joint reaction forces between the hybrid and the MSK models, both of which showed an increase from distal to proximal joints and a major difference at the DIP joint. The negligible differences between the hybrid and the MSK model may be explained by the use of different assumptions in the two numerical approaches, such as non-deformable bodies in the MSK model versus a more accurate representation of bone and cartilage in the hybrid model. Lastly, joint contact areas predicted in the hybrid model showed similar values to those of the MSK model and literature data (Moran et al. 1985).

The hybrid model proposes a new tendon force transmission based on a tendon-pulley system, where both flexor and extensor tendons slid in annular pulleys. This yielded estimations of the ratio of flexor tendon forces to fingertip force that were consistent with in-vivo measurements found in the literature (Schuind et al. 1992; Dennerlein et al. 1998; Kursa et al. 2005) and with MSK results, thus validating this approach (Table 3). In a previous study (Harih 2019), the DIP joint was driven by a concentrated force at the end of a wire connector which modelled the distal part of the flexor tendon. The same approach has been used in some foot FE models (Isvilanonda et al. 2012; Morales-Orcajo et al. 2015; Wang et al. 2016), with tendons crossing several joints and the tendon final insertion attached to the bone.

The choice of material properties in the hybrid model was based on several factors. Sensitivity analysis (see Supplementary Material B) showed that bone representation had an impact on joint contact pressures. Distinguishing between cortical and cancellous bone ensured here that the structure was rigid enough for good transmission of stresses between cartilage layers and bones. This suggests that piecewise assigning of linear-elastic material properties to bones, by calculating the density of the CT-scan gray value of each element, better matches the real microarchitecture of the bone. Cartilage was represented here as a monophasic time-independent hyperelastic material that could handle large deformations greater than 5%. Although this did not account for either poroelastic behaviour or fluid matrix interactions such as osmotic swelling or mechanical exudation of interstitial fluid (Halloran et al. 2012), hyperelastic models are deemed adequate to characterise the equilibrium response of cartilage (Brown et al. 2009).

The calculation of mean contact pressures for the maximal strength grip task performed by six subjects showed significant differences among them. For two subjects (4 and 9), mean contact pressures resulted in greater values for the DIP joint than for PIP and MCP joints. For the index finger, several studies have shown that OA is more frequent in the DIP joint than in the proximal joints (Caspi et al. 2001; Dahaghin et al. 2005). It can therefore be concluded that cumulative excessive stresses acting on joints should lead to the occurrence and development of OA, consistent with previous findings (Guilak 2011; Buckwalter et al. 2013). In contrast, the remaining four subjects (1, 2, 3 and 7) showed higher mean contact pressures in the MCP joint than in the PIP and DIP joints. Studies have found that the MCP joint is the most subject to OA development during maximal strength tasks (Jensen et al. 1999), while the DIP joint is the most sensitive under precision repetitive grip tasks (Lehto et al. 1990). Furthermore, to perform the maximal strength grip task, different neuromuscular strategies were employed by the subjects. Since these strategies activated the muscles in varying ways, they resulted in varying joint contact pressures. In subjects 4 and 9, greater mean contact pressures at the distal joint were induced by higher FDP muscular activity resulting in higher FDP tendon force. In subject 7, greater mean contact pressures at proximal and metacarpophalangeal joints were due to higher FDS and RI muscular activities resulting in higher FDS and RI tendon forces.

The mean contact pressures obtained in the hybrid simulation reached 8.0±1.4 MPa at the MCP joint (Table 5), which could indicate tissue consolidation. Indeed, this value was in the range of those moderate normal loadings needed for cartilage development and renewal, and to maintain functional integrity (Vanwanseele et al. 2002), thus keeping cartilage healthy (Parkkinen et al. 1992; Clements et al. 2001). However, peak contact pressures at DIP, PIP and MCP joints (higher than 15 MPa) corresponded to an excessive mechanical load which could therefore cause chondrocyte death and extracellular matrix damage (Torzilli et al. 1999), thus leading to OA initiation. It should be noted that this study examined an extreme force intensity of one of the most common techniques for manipulating objects, the pinch grip. While a pinch strength of 10 N will actually suffice for 90% of daily living activities (Hunter et al. 1978), the simulated pinch strength here was more than 5 times higher, with an experimental fingertip force of 66.2 ± 13.3 N. Thus, the task studied here could be considered as a worst-case for which the conditions of OA occurrence were assessed and evaluated.

The hybrid method presented in this article offers access to individual subjects' local stress distribution in index finger joints through a non-invasive evaluation. It can be applied and extended to the complete hand to simulate tasks such as the power grip and to potentially link the mechanical determinants and consequences of diseases such as OA. A deeper understanding of the biomechanics of the hand related to joint disease occurrence could provide the groundwork to improve surgical procedures, such as arthroplasty, through more effective numerical models.

Acknowledgment

The authors wish to thank André Jacques for his assistance with the numerical simulations.

Conflict of Interest Statement

No benefits in any form have been or will be received from a commercial party related directly or indirectly to the subject of this manuscript.

References

An KN, Chao EY, Cooney WP, Linscheid RL. 1979. Normative model of human hand for biomechanical analysis. J Biomech. 12(10):775–788.

Anderson AE, Ellis BJ, Maas SA, Weiss JA. 2010. Effects of idealized joint geometry on finite element predictions of cartilage contact stresses in the hip. J Biomech. 43(7):1351–1357.

Andriacchi TP, Koo S, Scanlan SF. 2009. Gait mechanics influence healthy cartilage morphology and osteoarthritis of the knee. J Bone Joint Surg Am. 91 Suppl 1:95–101.

Bardo A, Vigouroux L, Kivell TL, Pouydebat E. 2018. The impact of hand proportions on tool grip abilities in humans, great apes and fossil hominins: A biomechanical analysis using musculoskeletal simulation. J Hum Evol. 125:106–121.

Barry AJ, Murray WM, Kamper DG. 2018. Development of a dynamic index finger and thumb model to study impairment. J Biomech. 77:206–210.

Besier TF, Gold GE, Beaupré GS, Delp SL. 2005. A modeling framework to estimate patellofemoral joint cartilage stress in vivo. Med Sci Sports Exerc. 37(11):1924–1930.

Brown CP, Nguyen TC, Moody HR, Crawford RW, Oloyede A. 2009. Assessment of common hyperelastic constitutive equations for describing normal and osteoarthritic articular cartilage. Proc Inst Mech Eng [H]. 223(6):643–652.

Buckwalter JA, Anderson DD, Brown TD, Tochigi Y, Martin JA. 2013. The Roles of Mechanical Stresses in the Pathogenesis of Osteoarthritis: Implications for Treatment of Joint Injuries. Cartilage. 4(4):286–294.

Burkhart TA, Andrews DM, Dunning CE. 2013. Finite element modeling mesh quality, energy balance and validation methods: a review with recommendations associated with the modeling of bone tissue. J Biomech. 46(9):1477–1488.

Butz KD, Merrell G, Nauman EA. 2012a. A biomechanical analysis of finger joint forces and stresses developed during common daily activities. Comput Methods Biomech Biomed Engin. 15(2):131–140.

Butz KD, Merrell G, Nauman EA. 2012b. A three-dimensional finite element analysis of finger joint stresses in the MCP joint while performing common tasks. HAND. 7(3):341–345.

Caspi D, Flusser G, Farber I, Ribak J, Leibovitz A, Habot B, Yaron M, Segal R. 2001. Clinical, radiologic, demographic, and occupational aspects of hand osteoarthritis in the elderly. Semin Arthritis Rheum. 30(5):321–331.

Cheung JT-M, Zhang M, Leung AK-L, Fan Y-B. 2005. Three-dimensional finite element analysis of the foot during standing--a material sensitivity study. J Biomech. 38(5):1045–1054.

Choi H-H, Hwang S-M, Kang YH, Kim J, Kang BS. 2002. Comparison of Implicit and Explicit Finite-Element Methods for the Hydroforming Process of an Automobile Lower Arm. Int J Adv Manuf Technol. 20(6):407–413.

Clements KM, Bee ZC, Crossingham GV, Adams MA, Sharif M. 2001. How severe must repetitive loading be to kill chondrocytes in articular cartilage? Osteoarthritis Cartilage. 9(5):499–507.

Completo A, Nascimento A, Girão AF, Fonseca F. 2018. Biomechanical evaluation of pyrocarbon proximal interphalangeal joint arthroplasty: An in-vitro analysis. Clin Biomech Bristol Avon. 52:72–78.

Dahaghin S, Bierma-Zeinstra SMA, Ginai AZ, Pols H a. P, Hazes JMW, Koes BW. 2005. Prevalence and pattern of radiographic hand osteoarthritis and association with pain and disability (the Rotterdam study). Ann Rheum Dis. 64(5):682–687.

Dennerlein JT, Diao E, Mote CD, Rempel DM. 1998. Tensions of the flexor digitorum superficialis are higher than a current model predicts. J Biomech. 31(4):295–301.

D'Lima DD, Patil S, Steklov N, Slamin JE, Colwell CW. 2006. Tibial Forces Measured In Vivo After Total Knee Arthroplasty. J Arthroplasty. 21(2):255–262.

Fowler NK, Nicol AC. 2000. Interphalangeal joint and tendon forces: normal model and biomechanical consequences of surgical reconstruction. J Biomech. 33(9):1055–1062.

Gíslason MK, Stansfield B, Nash DH. 2010. Finite element model creation and stability considerations of complex biological articulation: The human wrist joint. Med Eng Phys. 32(5):523–531.

Goislard de Monsabert B, Rossi J, Berton E, Vigouroux L. 2012. Quantification of hand and forearm muscle forces during a maximal power grip task. Med Sci Sports Exerc. 44(10):1906–1916.

Goislard de Monsabert B, Vigouroux L, Bendahan D, Berton E. 2014. Quantification of finger joint loadings using musculoskeletal modelling clarifies mechanical risk factors of hand osteoarthritis. Med Eng Phys. 36(2):177–184.

Guilak F. 2011. Biomechanical factors in osteoarthritis. Best Pract Res Clin Rheumatol. 25(6):815–823.

Halloran JP, Sibole S, van Donkelaar CC, van Turnhout MC, Oomens CWJ, Weiss JA, Guilak F, Erdemir A. 2012. Multiscale mechanics of articular cartilage: potentials and challenges of coupling musculoskeletal, joint, and microscale computational models. Ann Biomed Eng. 40(11):2456–2474.

Halonen KS, Dzialo CM, Mannisi M, Venäläinen MS, de Zee M, Andersen MS. 2017. Workflow assessing the effect of gait alterations on stresses in the medial tibial cartilage - combined musculoskeletal modelling and finite element analysis. Sci Rep [Internet]. [accessed 2018 Sep 21] 7(1). http://www.nature.com/articles/s41598-017-17228-x

Harih G. 2019. Development of a Tendon Driven Finger Joint Model Using Finite Element Method. In: Cassenti DN, editor. Adv Hum Factors Simul Model [Internet]. Vol. 780. Cham: Springer International Publishing; [accessed 2018 Sep 27]; p. 463–471. http://link.springer.com/10.1007/978-3-319-94223-0_44

Hashizume H, Akagi T, Watanabe H, Inoue H, Ogura T. 1994. Stress Analysis of PIP Joints using the Three-Dimensional Finite Element Method. In: Schuind F, An KN, Cooney WP, Garcia-Elias M, editors. Adv Biomech Hand Wrist [Internet]. Boston, MA: Springer US; [accessed 2018 Sep 27]; p. 237–244. http://link.springer.com/10.1007/978-1-4757-9107-5_21

Henak CR, Anderson AE, Weiss JA. 2013. Subject-specific analysis of joint contact mechanics: application to the study of osteoarthritis and surgical planning. J Biomech Eng. 135(2):021003.

Hunter J, Schneider L, Mackin E, Bell J. 1978. Rehabilitation of the hand. St Louis: Mosby.

Isvilanonda V, Dengler E, Iaquinto JM, Sangeorzan BJ, Ledoux WR. 2012. Finite element analysis of the foot: model validation and comparison between two common treatments of the clawed hallux deformity. Clin Biomech Bristol Avon. 27(8):837–844.

Jensen V, Bøggild H, Johansen JP. 1999. Occupational use of precision grip and forceful gripping, and arthrosis of finger joints: a literature review. Occup Med Oxf Engl. 49(6):383–388.

Kursa K, Diao E, Lattanza L, Rempel D. 2005. In vivo forces generated by finger flexor muscles do not depend on the rate of fingertip loading during an isometric task. J Biomech. 38(11):2288–2293.

Lehto TU, Rönnemaa TE, Aalto TV, Helenius HY. 1990. Roentgenological arthrosis of the hand in dentists with reference to manual function. Community Dent Oral Epidemiol. 18(1):37–41.

McQuillan TJ, Kenney D, Crisco JJ, Weiss A-P, Ladd AL. 2016. Weaker Functional Pinch Strength Is Associated With Early Thumb Carpometacarpal Osteoarthritis. Clin Orthop. 474(2):557–561.

Minami A, An KN, Cooney WP, Linscheid RL, Chao EY. 1985. Ligament stability of the metacarpophalangeal joint: a biomechanical study. J Hand Surg. 10(2):255–260.

Morales-Orcajo E, Bayod J, Becerro-de-Bengoa-Vallejo R, Losa-Iglesias M, Doblare M. 2015. Influence of first proximal phalanx geometry on hallux valgus deformity: a finite element analysis. Med Biol Eng Comput. 53(7):645–653.

Moran JM, Hemann JH, Greenwald AS. 1985. Finger joint contact areas and pressures. J Orthop Res Off Publ Orthop Res Soc. 3(1):49–55.

Napier JR. 1956. THE PREHENSILE MOVEMENTS OF THE HUMAN HAND. J Bone Joint Surg Br. 38-B(4):902–913.

Parkkinen JJ, Lammi MJ, Helminen HJ, Tammi M. 1992. Local stimulation of proteoglycan synthesis in articular cartilage explants by dynamic compression in vitro. J Orthop Res Off Publ Orthop Res Soc. 10(5):610–620.

Rhee RY, Reading G, Wray RC. 1992. A biomechanical study of the collateral ligaments of the proximal interphalangeal joint. J Hand Surg. 17(1):157–163.

Rho JY, Tsui TY, Pharr GM. 1997. Elastic properties of human cortical and trabecular lamellar bone measured by nanoindentation. Biomaterials. 18(20):1325–1330.

Rikli DA, Honigmann P, Babst R, Cristalli A, Morlock MM, Mittlmeier T. 2007. Intra-articular pressure measurement in the radioulnocarpal joint using a novel sensor: in vitro and in vivo results. J Hand Surg. 32(1):67–75.

Robson MD, Hodgson RJ, Herrod NJ, Tyler JA, Hall LD. 1995. A combined analysis and magnetic resonance imaging technique for computerised automatic measurement of cartilage thickness in the distal interphalangeal joint. Magn Reson Imaging. 13(5):709–718.

Schuind F, Garcia-Elias M, Cooney WP, An KN. 1992. Flexor tendon forces: in vivo measurements. J Hand Surg. 17(2):291–298.

Synek A, Pahr DH. 2016. The effect of the extensor mechanism on maximum isometric fingertip forces: A numerical study on the index finger. J Biomech. 49(14):3423–3429.

Torzilli PA, Grigiene R, Borrelli J, Helfet DL. 1999. Effect of impact load on articular cartilage: cell metabolism and viability, and matrix water content. J Biomech Eng. 121(5):433–441.

Vanwanseele B, Eckstein F, Knecht H, Stüssi E, Spaepen A. 2002. Knee cartilage of spinal cord–injured patients displays progressive thinning in the absence of normal joint loading and movement. Arthritis Rheum. 46(8):2073–2078.

Vergara M, Sancho-Bru JL, Gracia-Ibáñez V, Pérez-González A. 2014. An introductory study of common grasps used by adults during performance of activities of daily living. J Hand Ther Off J Am Soc Hand Ther. 27(3):225–233; quiz 234.

Wang Y, Wong DW-C, Zhang M. 2016. Computational Models of the Foot and Ankle for Pathomechanics and Clinical Applications: A Review. Ann Biomed Eng. 44(1):213–221.

Wright V, Dowson D. 1976. Lubrication and cartilage. J Anat. 121(Pt 1):107–118.

Figure Captions

Figure 1. Hybrid musculoskeletal-finite element model applied to the index finger for the estimation of joint contact pressure during a static maximal strength pinch grip task. The musculoskeletal model applied to six subjects estimated tendon and joint forces from motion capture and force data through an inverse dynamic approach. The finite element model based on medical imaging data and including all the major structures of the index finger was driven by tendon forces of the musculoskeletal model. This hybrid approach validated by comparison with experimental data and musculoskeletal results yielded mean and maximal contact pressures at the three index finger joints.

Figure 2. Pulp pinch grip posture and experimental acquisition system. A motion capture system with spherical markers on bony landmarks and an axial force sensor between the thumb and index fingertips were used.

Figure 3. (A) Index finger finite element model of the hybrid approach including bones, cartilage, tendons, annular pulleys and ligaments. Cartilage in green was obtained by extrusion of the bone surfaces with wedge elements. Tendons and annular pulleys in light blue and grey, respectively, were modelled with beam and shell elements, respectively. Ligaments in dark blue were represented by multiple non-linear spring elements. The truncated metacarpal bone was fully constrained and the fingertip restricted to one degree of freedom (DoF) resulting in an external fingertip reaction force ($\overrightarrow{F_{ext}}$). Datasets of tendon forces ($\overrightarrow{F_{musc}}$) were applied along the last segment of each tendon. (B) Material properties distribution between cortical (in light grey) and cancellous bone (in black) on a section of the index finger bones.

Figure 4. Von Mises stress distribution of the index finger and contact pressure distribution at distal interphalangeal (DIP), proximal interphalangeal (PIP) and metacarpophalangeal (MCP) joints during a static maximal strength pinch grip task applying one dataset of tendon forces.

Tables

Table 1. Material properties and element types of the index finger hybrid finite element model

Component	Element type	Constitutive model	Constants
Cortical bone	Tetrahedral	Linear elastic	E=18 GPa; ν=0.2
Cancellous bone	Tetrahedral	Linear elastic	E=300 MPa; ν=0.25
Cartilage	Wedge	Hyper-elastic 3rd order Ogden	μ_1=-4527; α_1=-4.98 μ_2=2228; α_2=5.43 μ_3=2300; α_3=4.55 D_1=D_2= D_3=0
Tendons	Tension-only beam	Linear elastic	E=3 GPa; ν=0.3
Pulleys	Shell	Linear elastic	E=1 GPa; ν=0.3
Ligaments	Tension-only connector	Non-linear elastic	From 40 N/mm to 150 N/mm

Table 2. Mesh quality metrics of the hybrid finite element model

Mesh quality metric	Assessment criteria	Accurate elements
Jacobian elements	> 0.2	94%
Aspect ratio	< 3	96%
Max angles	< 120°	99%

Table 3. Comparison of ratios of tendon force to external fingertip force during pinch grip between MSK model, hybrid model and in-vivo measurements reported in the literature

	FDP	FDS
MSK model	1.7	2.4
Hybrid model	2.0	2.9
Schuind et al.	7.9 ± 6.3	1.7 ± 1.5
Denenrlein et al.	--	3.3 ± 1.4
Kursa et al.	2.4 ± 0.7	1.5 ± 1.0

Table 4. Force values obtained from musculoskeletal and hybrid models of the index finger. External fingertip force and joint reaction force in distal interphalangeal (DIP), proximal interphalangeal (PIP) and metacarpophalangeal (MCP) joints from the two models are compared.

	External fingertip force (N)	DIP joint reaction force (N)	PIP joint reaction force (N)	MCP joint reaction force (N)
MSK model	66.2 ± 13.3	125.5 ± 87.6	324.4 ± 144.4	609.6 ± 161.8
Hybrid model	54.8	193.5	418.6	718.2

Table 5. Cartilage contact pressures at distal interphalangeal (DIP), proximal interphalangeal (PIP) and metacarpophalangeal (MCP) joints estimated by the hybrid model for each of the six subjects and for the average. External fingertip force produced by the hybrid model.

		Subject number						Average
		1	2	3	4	7	9	
Cartilage contact pressure (MPa)	DIP joint	$\sigma_{\max} = 19.8$ $\sigma_{\text{mean}} = 4.8$	$\sigma_{\max} = 26.7$ $\sigma_{\text{mean}} = 6.2$	$\sigma_{\max} = 26.8$ $\sigma_{\text{mean}} = 5.7$	$\sigma_{\max} = 31.7$ $\sigma_{\text{mean}} = 7.1$	$\sigma_{\max} = 32.2$ $\sigma_{\text{mean}} = 7.3$	$\sigma_{\max} = 44.3$ $\sigma_{\text{mean}} = 12.2$	$\sigma_{\max} = 33.0$ $\sigma_{\text{mean}} = 6.6$
	PIP joint	$\sigma_{\max} = 22.8$ $\sigma_{\text{mean}} = 5.9$	$\sigma_{\max} = 27.4$ $\sigma_{\text{mean}} = 6.6$	$\sigma_{\max} = 31.9$ $\sigma_{\text{mean}} = 7.2$	$\sigma_{\max} = 24.2$ $\sigma_{\text{mean}} = 5.8$	$\sigma_{\max} = 42.2$ $\sigma_{\text{mean}} = 9.2$	$\sigma_{\max} = 42.6$ $\sigma_{\text{mean}} = 7.5$	$\sigma_{\max} = 33.3$ $\sigma_{\text{mean}} = 7.8$
	MCP joint	$\sigma_{\max} = 28.9$ $\sigma_{\text{mean}} = 6.8$	$\sigma_{\max} = 29.1$ $\sigma_{\text{mean}} = 7.1$	$\sigma_{\max} = 35.9$ $\sigma_{\text{mean}} = 8.9$	$\sigma_{\max} = 26.1$ $\sigma_{\text{mean}} = 6.6$	$\sigma_{\max} = 44.3$ $\sigma_{\text{mean}} = 10.0$	$\sigma_{\max} = 38.4$ $\sigma_{\text{mean}} = 8.6$	$\sigma_{\max} = 40.4$ $\sigma_{\text{mean}} = 9.5$
External fingertip force (N)		$F_{\text{exp}} = 42.5$ $F_{sim} = 36.6$	$F_{\text{exp}} = 62.4$ $F_{sim} = 45.7$	$F_{\text{exp}} = 65.2$ $F_{sim} = 48.3$	$F_{\text{exp}} = 53.5$ $F_{sim} = 39.7$	$F_{\text{exp}} = 78.4$ $F_{sim} = 59.6$	$F_{\text{exp}} = 64.7$ $F_{sim} = 47.6$	$F_{\text{exp}} = 66.2$ $F_{sim} = 54.8$

Supplementary Material A. Tendon forces for the index finger derived from the musculoskeletal model for each of the ten subjects (in N). In bold, the six subjects involved in the analysis.

	FDP	FDS	LU	RI	UI	EDC	EDI
Subject 1	**71,6**	**126,9**	**5,7**	**117,7**	**0,0**	**50,3**	**64,6**
Subject 2	**93,9**	**123,5**	**4,4**	**139,2**	**0,0**	**59,8**	**76,8**
Subject 3	**84,3**	**94,6**	**14,7**	**194,9**	**0,0**	**90,8**	**116,7**
Subject 4	**125,8**	**49,1**	**0,0**	**152,4**	**0,0**	**44,5**	**57,1**
Subject 5	99,7	210,1	0,0	149,2	0,0	67,2	86,4
Subject 6	113,8	281,1	4,2	262,1	0,0	141,0	181,1
Subject 7	**107,9**	**234,9**	**0,0**	**190,1**	**0,0**	**79,2**	**101,7**
Subject 8	102,1	177,4	12,9	245,4	0,0	124,6	160,0
Subject 9	**217,2**	**46,2**	**9,6**	**161,3**	**0,0**	**72,1**	**92,6**
Subject 10	81,6	236,3	0,0	199,6	0,0	126,4	162,4
Average	109,8	158,0	5,1	181,2	0,0	85,6	110,0
SD	41,0	82,2	5,6	46,3	0,0	34,1	43,8

Supplementary Material B. Sensitivity analysis

A sensitivity analysis was performed to investigate the effect of bone material properties and tendon force on the model prediction results. The bone was modelled with three different types of material properties:

- rigid behaviour;
- a single Young's modulus value for all the bone averaged between cortical and cancellous elasticity values;
- distinct cortical and cancellous bone regions (Fig. 3(B))

Tendon force analysis included six cases of tendon force: 100%, 90%, 80%, 70%, 60% and 50% from the baseline values in Supplementary Material A to simulate submaximal grip force levels.

Representing the bone with either rigid behaviour or a single Young's modulus value for all the bone averaged between cortical and cancellous elasticity values led respectively to 11% and 3% higher mean contact pressure at the PIP joint than when distinct cortical and cancellous bone regions were used. All three representations of materials yielded the same values for fingertip force estimation and joint forces. Reducing tendon forces resulted in decreased joint contact pressure, fingertip force, and joint forces. In particular, fingertip force decreased linearly with tendon force (linear correlation of 0.47, R^2=0.99) from 54.8 N at maximal tendon force to 25.8 N at halved tendon force. Mean contact pressure also decreased linearly with tendon force (linear correlation of 0.59), from 9.5 MPa, 7.8 MPa, 6.6 MPa at maximal tendon force to 5.5 MPa, 4.9 MPa, 4.2 MPa at halved tendon force for MCP, PIP and DIP joint, respectively.

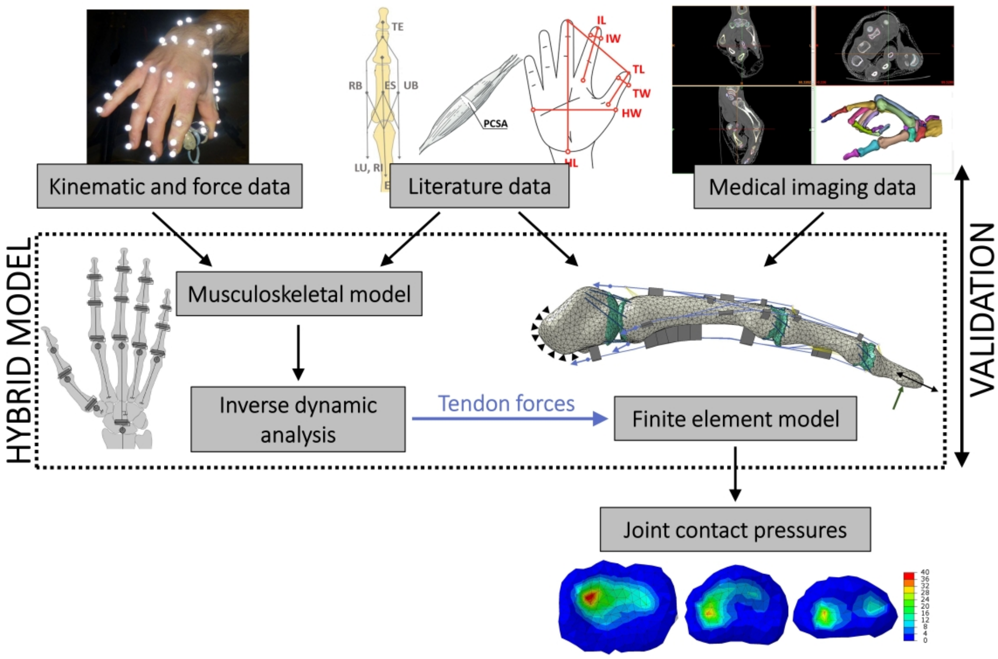

Figure 1. Hybrid musculoskeletal-finite element model applied to the index finger for the estimation of joint contact pressure during a static maximal strength pinch grip task. The musculoskeletal model applied to six subjects estimated tendon and joint forces from motion capture and force data through an inverse dynamic approach. The finite element model based on medical imaging data and including all the major structures of the index finger was driven by tendon forces of the musculoskeletal model. This hybrid approach validated by comparison with experimental data and musculoskeletal results yielded mean and maximal contact pressures at the three index finger joints.

569x379mm (300 x 300 DPI)

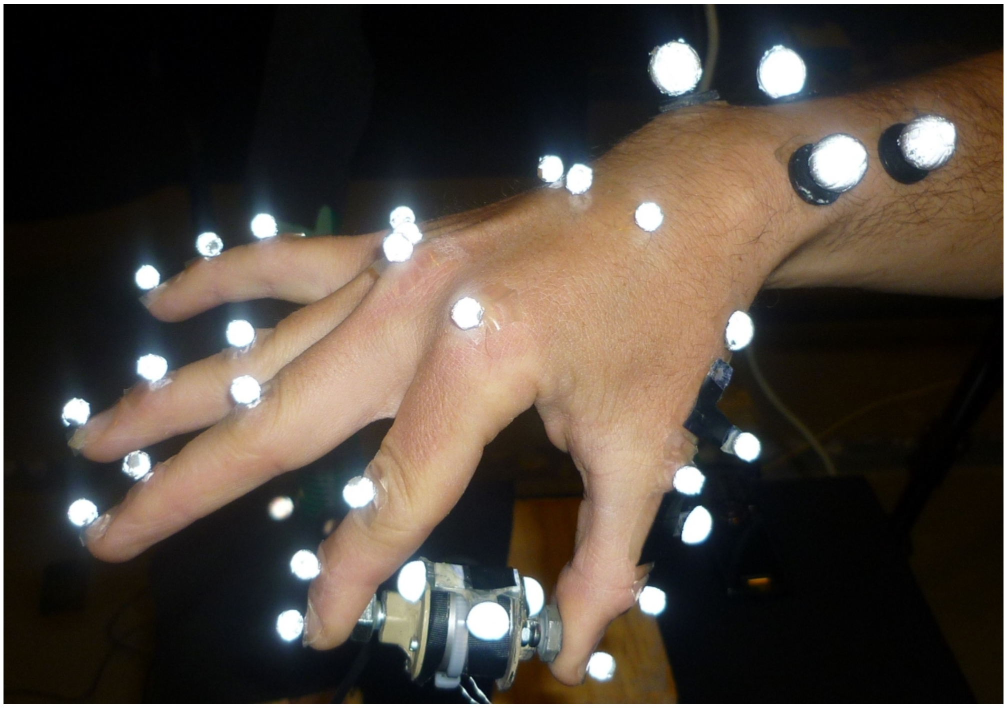

Figure 2. Pulp pinch grip posture and experimental acquisition system. A motion capture system with spherical markers on bony landmarks and an axial force sensor between the thumb and index fingertips were used.

244x171mm (300 x 300 DPI)

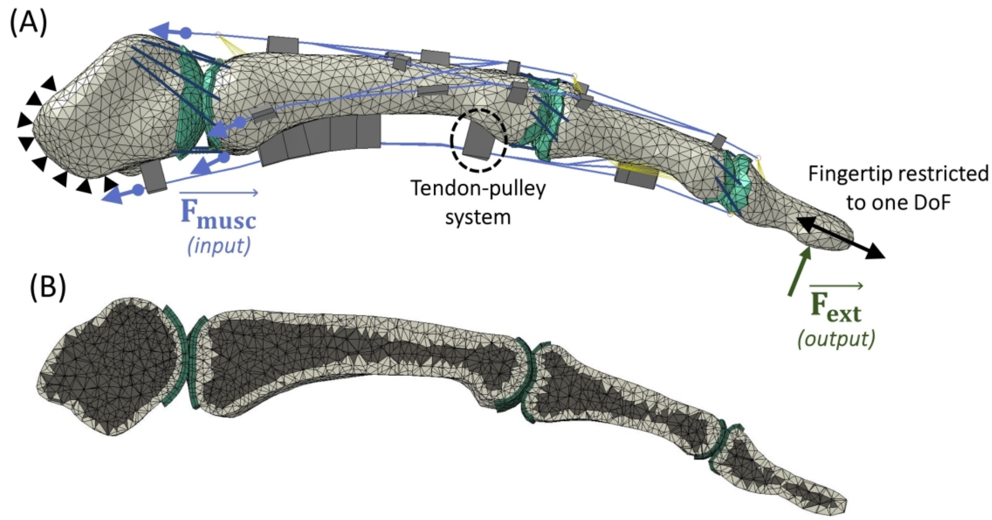

Figure 3. (A) Index finger finite element model of the hybrid approach including bones, cartilage, tendons, annular pulleys and ligaments. Cartilage in green was obtained by extrusion of the bone surfaces with wedge elements. Tendons and annular pulleys in light blue and grey, respectively, were modelled with beam and shell elements, respectively. Ligaments in dark blue were represented by multiple non-linear spring elements. The truncated metacarpal bone was fully constrained and the fingertip restricted to one degree of freedom (DoF) resulting in an external fingertip reaction force (Fext). Datasets of tendon forces (Fmusc) were applied along the last segment of each tendon. (B) Material properties distribution between cortical (in light grey) and cancellous bone (in black) on a section of the index finger bones.

293x156mm (300 x 300 DPI)

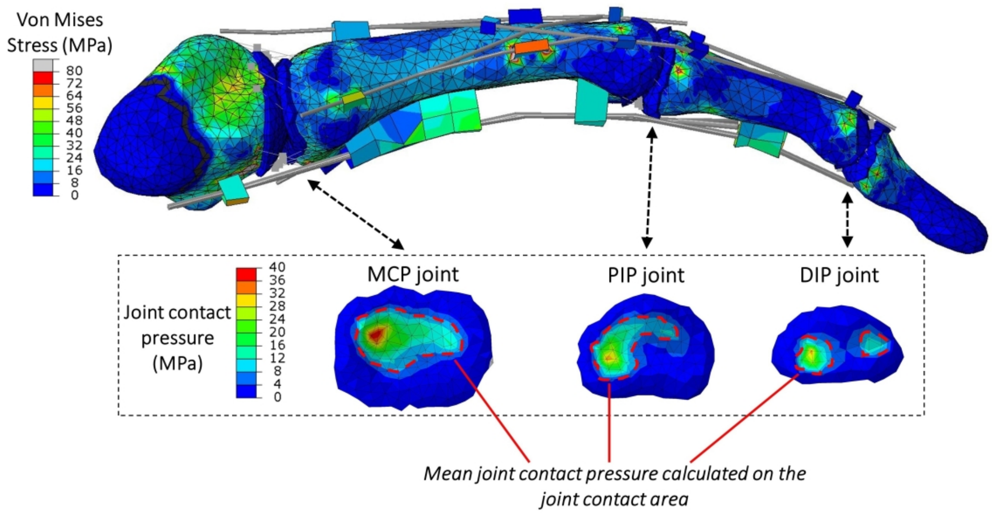

Figure 4. Von Mises stress distribution of the index finger and contact pressure distribution at distal interphalangeal (DIP), proximal interphalangeal (PIP) and metacarpophalangeal (MCP) joints during a static maximal strength pinch grip task applying one dataset of tendon forces.

297x155mm (300 x 300 DPI)